The Astrophysical Journal, 930:5 (10pp), 2022 May 1 https://doi.org/10.3847/1538-4357/ac6109


# A Quasar Shedding Its Dust Cocoon at Redshift 2

Weimin Yi[1,2,3], W. N. Brandt[2,4,5], Q. Ni[2], Luis C. Ho[6,7], Bin Luo[8], Wei Yan[2], D. P. Schneider[2,4], Jeremiah D. Paul[9], Richard M. Plotkin[9], Jinyi Yang[10], Feige Wang[10], Zhicheng He[11], Chen Chen[12], Xue-Bing Wu[6,7], and Jin-Ming Bai[1,3]

[1] Yunnan Observatories, Chinese Academy of Sciences, Kunming, 650216, People's Republic of China; ywm@ynao.ac.cn
[2] Department of Astronomy & Astrophysics, The Pennsylvania State University, 525 Davey Lab, University Park, PA 16802, USA
[3] Key Laboratory for the Structure and Evolution of Celestial Objects, Chinese Academy of Sciences, Kunming 650216, People's Republic of China
[4] Institute for Gravitation and the Cosmos, The Pennsylvania State University, University Park, PA 16802, USA
[5] Department of Physics, 104 Davey Laboratory, The Pennsylvania State University, University Park, PA 16802, USA
[6] Kavli Institute for Astronomy and Astrophysics, Peking University, Beijing 100871, People's Republic of China
[7] Department of Astronomy, Peking University, Yi He Yuan Lu 5, Hai Dian District, Beijing 100871, People's Republic of China
[8] School of Astronomy and Space Science, Nanjing University, Nanjing, Jiangsu 210093, People's Republic of China
[9] Department of Physics, University of Nevada, Reno, NV 89557, USA
[10] Steward Observatory, University of Arizona, Tucson, AZ 85721-0065, USA
[11] CAS Key Laboratory for Research in Galaxies and Cosmology, Department of Astronomy, University of Science and Technology of China, Hefei, Anhui 230026, People's Republic of China
[12] School of Physics & Astronomy, Sun Yat-Sen University, Zhuhai 519000, People's Republic of China
*Received 2021 December 15; revised 2022 March 11; accepted 2022 March 14; published 2022 April 28*

## Abstract

We present the first near-IR spectroscopy and joint analyses of multiwavelength observations for SDSS J082747.14+425241.1, a dust-reddened, weak broad emission-line quasar (WLQ) undergoing a remarkable broad-absorption line (BAL) transformation. The systemic redshift is more precisely measured to be $z = 2.070 \pm 0.001$ using H$\beta$ compared to $z = 2.040 \pm 0.003$ using Mg II from the literature, signifying an extreme Mg II blueshift of $2140 \pm 530$ km s$^{-1}$ relative to H$\beta$. Using the H$\beta$-based single-epoch scaling relation with a systematic uncertainty of 0.3 dex, its black hole (BH) mass and Eddington ratio are estimated to be $M_{\rm BH} \sim 6.1 \times 10^8 M_\odot$ and $\lambda_{\rm Edd} \sim 0.71$, indicative of being in a rapidly accreting phase. Our investigations confirm the WLQ nature and the LoBAL → HiBAL transformation, along with a factor of 2 increase in the Mg II+Fe II emission strength and a decrease of 0.1 in $E(B-V)$ over two decades. The kinetic power of this LoBAL wind at $R \sim 15$ pc from its BH is estimated to be ∼43% of the Eddington luminosity, sufficient for quasar feedback upon its host galaxy albeit with an order-of-magnitude uncertainty. This quasar provides a clear example of the long-sought scenario where LoBAL quasars are surrounded by dust cocoons, and wide-angle nuclear winds play a key role in the transition of red quasars evolving into the commonly seen blue quasars.

*Unified Astronomy Thesaurus concepts:* Quasars (1319); Broad-absorption line quasar (183); Supermassive black holes (1663)

## 1. Introduction

Broad emission-line (BEL) blueshifts relative to systemic redshift are often seen in quasars and interpreted as evidence for quasar winds (e.g., Gaskell 1982; Richards et al. 2011; Xu et al. 2020; Yi et al. 2020; Zuo et al. 2020). As a comparison, broad-absorption lines (BALs; Weymann et al. 1991) are unambiguous evidence for outflows driven by quasars (quasar winds in short), presumably because of their extreme outflow properties that cannot be explained by any known stellar processes. There are two major BAL-type quasars, namely high-ionization BAL (HiBAL, typically traced by N V, C IV, and/or Si IV) and low-ionization BAL (LoBAL, typically traced by Mg II and/or Al III in addition to HiBAL species at the same velocity) quasars. The observed HiBAL/LoBAL fractions are ∼15%/∼1.5% based on optically identified quasar samples, but the intrinsic BAL fraction may be up to ∼40% after selection corrections (e.g., Allen et al. 2011).

Orientation and evolution are the two most widely accepted interpretations with respect to BAL phenomena. A growing number of studies have suggested that HiBAL and non-BAL quasars could represent different views of the same underlying quasar population, on the basis of both populations having many similarities in outflow and physical properties (e.g., Rankine et al. 2020; Xu et al. 2020; Yi et al. 2020; Liu et al. 2021). This finding is more consistent with the orientation than evolution in accounting for the HiBAL phenomena. Conversely, BAL (particularly LoBAL) quasars have also been widely interpreted as being in a special evolutionary phase, in that high-column-density BALs signify powerful winds predominantly driven by rapidly accreting SMBHs. Such powerful winds support the long-sought blowout scenario for the origin of the observed large population of blue quasars. The two interpretations of BAL phenomena may be reconciled when noticing that the orientation and evolution scenarios have been drawn mostly from HiBAL and LoBAL quasars, respectively.

There are evident differences between the HiBAL and LoBAL populations. Previous observations have established that reddening decreases from LoBAL, HiBAL, to non-BAL quasars (Richards et al. 2003). While BAL quasars appear to be a minority of the entire quasar population, the BAL fraction increases with the increase in reddening (e.g., Richards et al. 2003); in particular, some studies found that the observed BAL

fraction is strikingly higher in red quasars than in blue quasars ($\gtrsim$50% versus ∼15%; e.g., Urrutia et al. 2009; Fynbo et al. 2013). Interestingly, Hamann et al. (2019) revealed from a large sample that LoBAL quasars have on average larger velocities, higher column densities, and softer ionizing spectral energy distributions (SEDs) than HiBAL quasars, suggesting the presence of extremely powerful outflows in the LoBAL population. In addition, Yi et al. (2019a) discovered a remarkable time-dependent trend of BAL variability in a LoBAL sample, such that weakening BALs outnumber strengthening BALs on longer sampling timescales (see Figure 9 in that work). In comparison, this trend does not appear to hold in the HiBAL population (e.g., Filiz Ak et al. 2013; Wang et al. 2015; De Cicco et al. 2018; Rogerson et al. 2018).

The differences between the HiBAL and LoBAL populations above suggest an evolutionary path from red to blue quasars. Combined with BAL-variability studies from the literature, Yi & Timlin (2021) found an overall LoBAL → HiBAL/non-BAL transformation sequence along with a decrease in dust, shedding light on the evolutionary path from red to blue quasars, i.e., a substantial fraction of LoBAL quasars could be caught in the act of casting off their dust cocoons (e.g., Boroson & Meyers 1992; Voit et al. 1993; Glikman et al. 2012). Furthermore, this scenario lends support to the argument for dusty winds as the origin of quasar reddening (Calistro Rivera et al. 2021). However, some recent studies of luminous type 1 quasars found apparent diverging evidence: There are no significant differences in emission-line outflow properties between red and blue quasars that match in luminosity (e.g., Temple et al. 2019; Villar Martín et al. 2020; Fawcett et al. 2022).

Given the above statistical evidence for red quasars evolving into blue quasars and the lack of significant differences in emission-line outflow properties, it is meaningful to test the evolution path via individual objects, especially those in a special phase and/or having unambiguous quasar winds. These extreme cases can be used to extend the dynamic ranges of fundamental properties and relationships found in statistical studies. SDSS J082747.14+425241.1 (hereafter J0827) is one such example, characterized by remarkable BAL transitions occurring in Mg II, Al III, and C IV BAL species, which offers a unique opportunity to investigate BAL transformations. On the other hand, J0827 is a weak broad emission-line quasar (WLQ) whose nature remains poorly understood. A puzzle with WLQs is that they appear to be normal quasars in nearly every aspect except for their unusually weak high-ionization BELs and remarkable X-ray properties (e.g., Fan et al. 1999; Diamond-Stanic et al. 2009; Wu et al. 2012; Luo et al. 2015; Ni et al. 2018, 2020; Timlin et al. 2020). The coexistence of weak BELs and transient BALs in J0827 provides a natural laboratory to explore the underlying link.

In this work, we present new observational results and implications from joint analyses of optical/near-IR spectroscopy for this red quasar, which has extreme properties reported in previous studies. Throughout this work, a flat cosmology with $H_0 = 71\,\mathrm{km\,s^{-1}\,Mpc^{-1}}$, $\Omega_M = 0.27$, and $\Omega_\Lambda = 0.73$ is adopted.

## 2. Previous and New Observations

As reported in Yi et al. (2019b) and Yi & Timlin (2021), the four different-epoch spectra of this quasar from the Sloan Digital Sky Survey (SDSS; York et al. 2000) demonstrated gradual BAL disappearance in multiple ions from MJD = 52,266 to 57,063; as a comparison, later observations from MJD = 58,212 to 58,486 by the Low-Resolution Spectrograph 2 (LRS2; Chonis et al. 2014) mounted on the Hobby-Eberly Telescope (HET; Ramsey et al. 1998; Hill et al. 2021) and the GMOS mounted on the Gemini-North telescope clearly revealed the rapid emergence of a higher-velocity C IV BAL.

**Table 1**
Spectroscopic Observations of J0827

| Instrument Name | $\lambda/\Delta\lambda$ | Spectral Coverage ($\mu$m) | Exp (hr) | Observation Date (MJD) |
|---|---|---|---|---|
| (A) | | | | |
| SDSS | 1800 | 0.38–0.92 | 2.5 | 52,266 |
| SDSS | 1800 | 0.38–0.92 | 1.0 | 54,524 |
| BOSS | 1800 | 0.36–1.03 | 1.3 | 55,513 |
| BOSS | 1800 | 0.36–1.03 | 1.5 | 57,063 |
| HET/LRS2 | 2000 | 0.36–0.7 | 0.7 | 58,212 |
| HET/LRS2 | 2000 | 0.36–0.7 | 0.7 | 58,428 |
| Gemini/GMOS | 1200 | 0.37–1.03 | 2.5 | 58,486 |
| (B) | | | | |
| P200/TripleSpec | 2700 | 1.0–2.5 | 1.5 | 58,726 |
| Gemini/GNIRS | 800 | 1.0–2.5 | 2.0 | 58,920 |
| HET/LRS2 | 2000 | 0.36–0.7 | 0.7 | 59,140 |
| HET/LRS2 | 2000 | 0.36–0.7 | 0.7 | 59,498 |

**Note.** (A) Previous observations of this quasar (see Yi et al. 2019b; Yi & Timlin 2021). (B) New observations of this quasar in this work.

To trace the subsequent variability of this quasar, we obtained additional optical spectra using HET/LRS2. Unlike the discovery paper from Yi et al. (2019b), the new HET/LRS2 spectra in this work were processed by the pipeline including flux calibration (Davis et al. 2018; Indahl et al. 2019), with a typical uncertainty of ∼20% in the absolute flux calibration.

In order to more precisely determine its systemic redshift, we also performed near-IR spectroscopic observations of J0827 using the Palomar Hale 200 inch telescope (P200/TripleSpec; Wilson et al. 2004). TripleSpec provides a wavelength coverage from 1.0 to 2.5 $\mu$m at an average spectral resolution of ∼2700, allowing simultaneous observations in the $J/H/K$ bands. A slit width of 1″ and the ABBA dither pattern along the slit were chosen to improve the sky subtraction.

However, due to difficulties in analyzing the data with a relatively low signal-to-noise ratio (S/N) obtained from P200/TripleSpec, we requested additional, higher-S/N near-IR observations using the Gemini Near-IR Spectrograph (GNIRS) via the Fast Turnaround program at Gemini Observatory (PI: W. Yi). Observations of a standard star with coordinates close to the target were also executed to improve flux calibration and telluric correction. The Gemini spectra were processed using the Gemini IRAF package via standard techniques, which have an uncertainty range of 10%–20% in flux calibration because they were taken in a nonphotometric condition. The log of all the observations for this quasar analyzed in this study is shown in Table 1.

## 3. Observational Results

The remarkable optical properties of this quasar have been reported in Yi et al. (2019b) and partly revisited in Yi & Timlin (2021), which will be mentioned only in passing in this work.

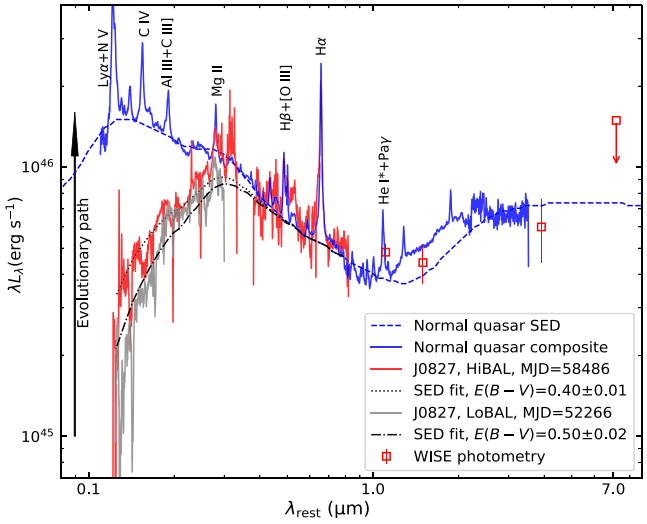


**Figure 1.** Comparisons between the LoBAL and non-BAL quasar composite spectra (scaled to the W1/W2/W3 fluxes of J0827). The squares are the photometric data from WISE. Here, only the two-epoch spectra of J0827 are shown to depict the LoBAL → HiBAL transformation along with a large decrease in reddening over the two epochs, consistent with the evolutionary path from red to blue quasars driven by quasar winds.

Here, we mainly focus on delivering new results based on the joint analyses of optical/near-IR spectroscopy.

### 3.1. Systemic Redshift

Both near-IR spectra obtained by P200/TripleSpec and Gemini/GNIRS show strong, broad H$\alpha$ emission lines; furthermore, the higher-S/N Gemini/GNIRS spectrum exhibited a narrow H$\beta$ component, producing a systemic redshift of $z = 2.070 \pm 0.001$, a value that is in excellent agreement with that determined by the narrow H$\alpha$ emission peak. Throughout this work, we use only the Gemini/GNIRS spectrum for the related analyses and visualization.

Noticeably, the H$\beta$-based systemic redshift is much higher than the Mg II-based systemic redshift $z \approx 2.040 \pm 0.003$ that was determined from optical spectroscopy, implying a large Mg II blueshift (see Section 3.4.2) and higher line-of-sight (LOS) velocities than previously reported for the two BALs, i.e., the newly emerged C IV BAL falls into the range of extremely high-velocity (0.1–0.2$c$) outflows (Rodríguez Hidalgo et al. 2020).

### 3.2. SED Properties

To complete the optical/near-IR spectroscopic data, we searched for mid-IR photometric detections from the WISE database (Wright et al. 2010, 2019) and found that J0827 was significantly detected (>5$\sigma$) in W1, W2, and W3, but only marginally (<3$\sigma$) in W4.

Of particular interest here is to investigate the SEDs and emission-line properties between this (red) quasar and normal (blue) quasars (see Figure 1). We construct the normal quasar composite spectrum from the literature (at $\lambda_{\rm rest} < 0.3\ \mu$m from Vanden Berk et al. 2001 and at $\lambda_{\rm rest} > 0.3\ \mu$m from Glikman et al. 2006). As shown in Figure 1, there are several dramatic differences: (1) J0827 is heavily reddened compared to the non-BAL quasar composite at $\lambda_{\rm rest} < 0.3\ \mu$m, confirming a large amount of dust in J0827. (2) The continuum of J0827 becomes bluer at MJD = 58,486 than that at MJD = 52,266, consistent with the evolutionary path from red to blue quasars. (3) There is no significant difference in H$\alpha$ emission between J0827 and the normal quasar composite, in agreement with the finding from Banerji et al. (2015). (4) The SED of J0827 appears to peak at $\lambda_{\rm rest} = 7\ \mu$m, a feature usually seen in red quasars. Although the W4-band detection for J0827 is marginal and sets only an upper limit, the excess emission at $\lambda_{\rm rest} = 7\ \mu$m likely exists in J0827 (see Section 4).

Assuming the scaled normal quasar SED (Richards et al. 2006) in Figure 1 is the intrinsic SED of J0827, we perform the SED fits at $0.13 < \lambda_{\rm rest} < 0.8\ \mu$m to quantify the change in continuum reddening over the two epochs. We choose the unusual reddening curve from Jiang et al. (2013) rather than the widely adopted Small Magellanic Cloud (SMC) reddening curve, as it can better reproduce the observed UV/optical continua (see Section 4). Specifically, we performed the spectral fit by modeling a reddened quasar SED to the relatively line-free windows identified by visual inspection, and the fitting uncertainties were generated by the standard deviations from the fits of 100 mock spectra via a Monte Carlo approach for both spectra.

### 3.3. Measurements from Near-IR Spectroscopy

We choose H$\beta$ as the BH-mass tracer throughout this work, given that it has been confirmed to be a robust virial BH-mass estimator in single-epoch scaling relations (Greene & Ho 2005; Du et al. 2014; Grier et al. 2017). In addition, previous studies revealed that the spectral region around H$\beta$ is much less affected by BEL blueshift, intrinsic reddening, and absorption than Mg II or C IV (e.g., Plotkin et al. 2015; Coatman et al. 2019; Yi et al. 2020). Recently, Yi et al. (2020) found observational evidence for BAL winds influencing the C IV and Mg II BELs more dramatically than the H$\beta$ BEL from a small LoBAL sample at $3 \lesssim z \lesssim 5$. In agreement with this effect, we find that J0827 shows a striking difference between the Mg II- and H$\beta$-based systemic redshifts ($z = 2.04$ versus $z = 2.07$), confirming our initial concern with using the observed Mg II BEL as a BH-mass tracer for this quasar (see Yi et al. 2019b). Therefore, H$\beta$ is the best-available tracer of BH mass for J0827. A general equation of the single-epoch scaling relation can be expressed as

$$\log\left[\frac{M_{\rm BH}}{M_\odot}\right] = a + b \times \log\left[\frac{\lambda L_\lambda}{10^{44}\ {\rm erg\ s^{-1}}}\right] + 2\log\left[\frac{\rm FWHM}{\rm km\ s^{-1}}\right]. \quad (1)$$

There are several parameter configuration sets ($a$, $b$) adopted in the literature to estimate the BH mass, depending on the specific calibration. To be consistent with previous WLQ studies (e.g., Luo et al. 2015; Plotkin et al. 2015; Ni et al. 2018), we use the same prescription ($a = 0.7$, $b = 0.5$ for H$\beta$) as Plotkin et al. (2015) to estimate the BH mass for this quasar. We first perform a local pseudo-continuum fit with a power-law function and an iron template from Boroson & Green (1992). We then subtract the fitted pseudo-continuum from the raw spectrum to obtain the emission lines of interest. For the emission-line fits, we adopt a similar prescription from the literature (Greene & Ho 2005), in which the velocity separation and dispersion across the narrow emission lines are tied to each other, and the amplitude ratios are fixed to 2.96 for [N II] $\lambda$6583/$\lambda$6548 and [O III] $\lambda$5007/$\lambda$4959. We do not

consider modeling the [S II] $\lambda6716/\lambda6731$ emission due to the apparent lack of such features imprinted on the near-IR spectrum. The broad-line region (BLR) component for H$\beta$ or H$\alpha$ is modeled with up to two Gaussians; however, unlike the modeling for narrow emission lines, we do not tie kinematics when modeling the broad H$\beta$ and H$\alpha$ emission.

The simultaneous spectral fit across these emission lines is shown in Figure 2. The FWHM of the BLR component of H$\beta$ is measured to be $3960 \pm 1090\,\mathrm{km\,s^{-1}}$ (the uncertainties are measured via a Monte Carlo approach through randomizations of spectral errors in the line-fitting window). The measurements may have larger uncertainties due to telluric absorption on the blue wing, but the total measurement error is still less than the systematic uncertainty of the scaling relation (typically 0.3 dex for H$\beta$) even considering this uncertainty. Because the above scaling relation has not been calibrated against reverberation mapping samples of BAL quasars, we adopt the systematic uncertainty for conservative purposes. The monochromatic luminosity ($\lambda L_\lambda$) at 5100 Å after correcting for Galactic extinction (Schlafly & Finkbeiner 2011) is measured to be $\approx 5.89 \times 10^{45}$ erg s$^{-1}$ for J0827. Because the scaled normal quasar SED is in good agreement with the observed SED at $0.4 < \lambda_{\rm rest} < 0.8\ \mu$m, we choose the unusual reddening curve in Jiang et al. (2013) with $E(\lambda - 1\ \mu\mathrm{m}) \approx 0.02$ mag at $\lambda = 0.51\ \mu$m to correct internal extinction, which yields the 5100 Å monochromatic luminosity of $\approx 6.0 \times 10^{45}$ erg s$^{-1}$ for J0827. Note that there is a degeneracy between the reddening and intrinsic SED shape. Combining all these pieces, the BH mass is then estimated to be $M_{\rm BH} = (6.1^{+3.8}_{-2.9}) \times 10^8 M_\odot$ according to Equation (1). This result is also consistent with that derived by H$\alpha$ ($\sim 4.5 \times 10^8 M_\odot$) using the prescription from Greene & Ho (2005). Consequently, the H$\beta$-based Eddington ratio is $\lambda_{\rm Edd} = 0.71^{+0.43}_{-0.33}$ with a bolometric correction factor of 9.26 (see Yi et al. 2020 and references therein), suggestive of being in a rapid accretion phase. The narrow-core component of [O III] is weak, perhaps due to shielding associated with dusty outflows (see Section 4.3).

### 3.4. New Results from Optical Spectra

The optical spectra of J0827 at MJD $\leqslant$ 58,486 were used in our previous studies for this quasar (Yi et al. 2019b; Yi & Timlin 2021). In this work, we have obtained two additional optical spectra from HET/LRS2 and present all the optical spectra in Figure 3 for an overview. Following Yi et al. (2019b), all the spectra are normalized using the power-law model to fit the local spectral regions that are visually identified to be free of emission and absorption features. For better visual clarity, we smooth all the optical spectra with a 15 pixel ($\sim$900 km s$^{-1}$) Savitzky–Golay filter window. This smoothing appears optimal for visual inspection.

The Balnicity index (BI; Weymann et al. 1991) is widely adopted to search for and characterize BALs. The BI, whose definition is similar to the rest-frame equivalent width (REW), can be expressed by the following integral:

$$\mathrm{BI} = \int_a^b \left[1 - \frac{f(v)}{0.9}\right] C dv, \qquad (2)$$

where $f(v)$ is the normalized flux; $C$ is set to zero and only becomes one when the term in the square bracket is continuously positive across a velocity interval of the specific choice, with a flux density less than 90% of the fitted

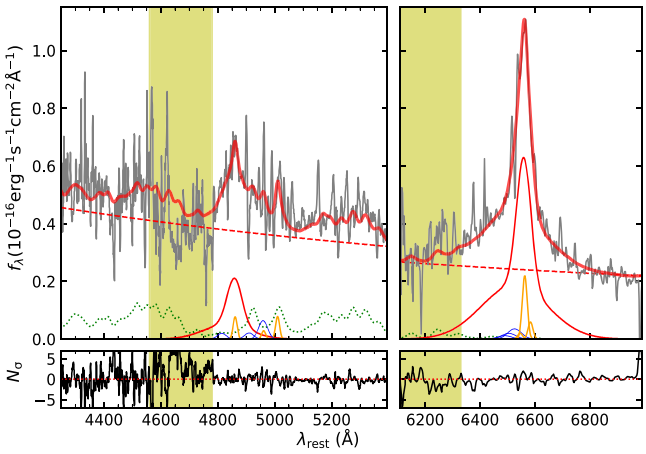


**Figure 2.** Spectral fits for the H$\beta$ (left) and H$\alpha$ (right) emission lines, in which the thick red lines are the models including the power-law continua (red dashed), the Fe II components (green dotted), the narrow-core components (orange), the broad-wing components (blue), and the BLR components (thin red). $N_\sigma$ in the bottom rows is the model-minus-data residual divided by the corresponding spectral error. Strong telluric absorption (yellow shaded) regions were masked during the fits.

continuum. $a$ and $b$ are the velocity integration limits, with the canonical values ($a = -3000$ and $b = -25{,}000$ km s$^{-1}$) set to avoid contamination by other ions. However, these limits should be modified in cases where the scientific goals include the investigations of intrinsic narrow absorption lines or extremely high-velocity outflows (e.g., Gibson et al. 2009; Rodríguez Hidalgo et al. 2020). We adopt a velocity interval of 1000 km s$^{-1}$ to allow the measurements for relatively narrow but intrinsic absorption features. Based on visual inspection of the nine-epoch spectra of J0827, $a$ and $b$ are set to be –40,000 and –10,000 km s$^{-1}$ for this quasar, within which we identified two distinct BALs whose flux-weighted centroid velocities are measured at $v_{\rm LOS} = 0.098 \pm 0.003c$ and $0.075 \pm 0.002c$ (the uncertainties are obtained from the minimum and maximum centroid velocities over the nine epochs; see the dashed and dotted lines in Figure 4), respectively.

#### 3.4.1. BAL Transformation

The definition of BI mentioned above is easy to understand, but one cannot use the BI measurements to determine whether the BALs over different epochs are physically connected. Although the analysis of BAL-complex troughs based on multiepoch spectra can alleviate this issue to some extent (e.g., Filiz Ak et al. 2013; Yi et al. 2019a), ambiguities cannot be eliminated without sufficient sampling epochs to trace the detailed BAL-profile variability over at least a few rest-frame years. This is particularly true in the case of J0827, where the BALs varied dramatically from epoch to epoch (see Figure 4); specifically, there are three BAL-like troughs meeting BI $> 0$ at MJD $= 57{,}063$, making the assessment of whether they arise from the same region difficult. Fortunately, the well-separated sampling epochs of J0827 over two decades, along with the simultaneous BAL disappearance and emergence, provide solid evidence that the gray and orange shaded BALs are physically distinct from each other, further in support of transverse motion dominating the BAL disappearance/emergence. Therefore, we use the two BAL distances ($\sim$0.5 and $\sim$15 pc from the SMBH; see Yi et al. 2019b) throughout this work.

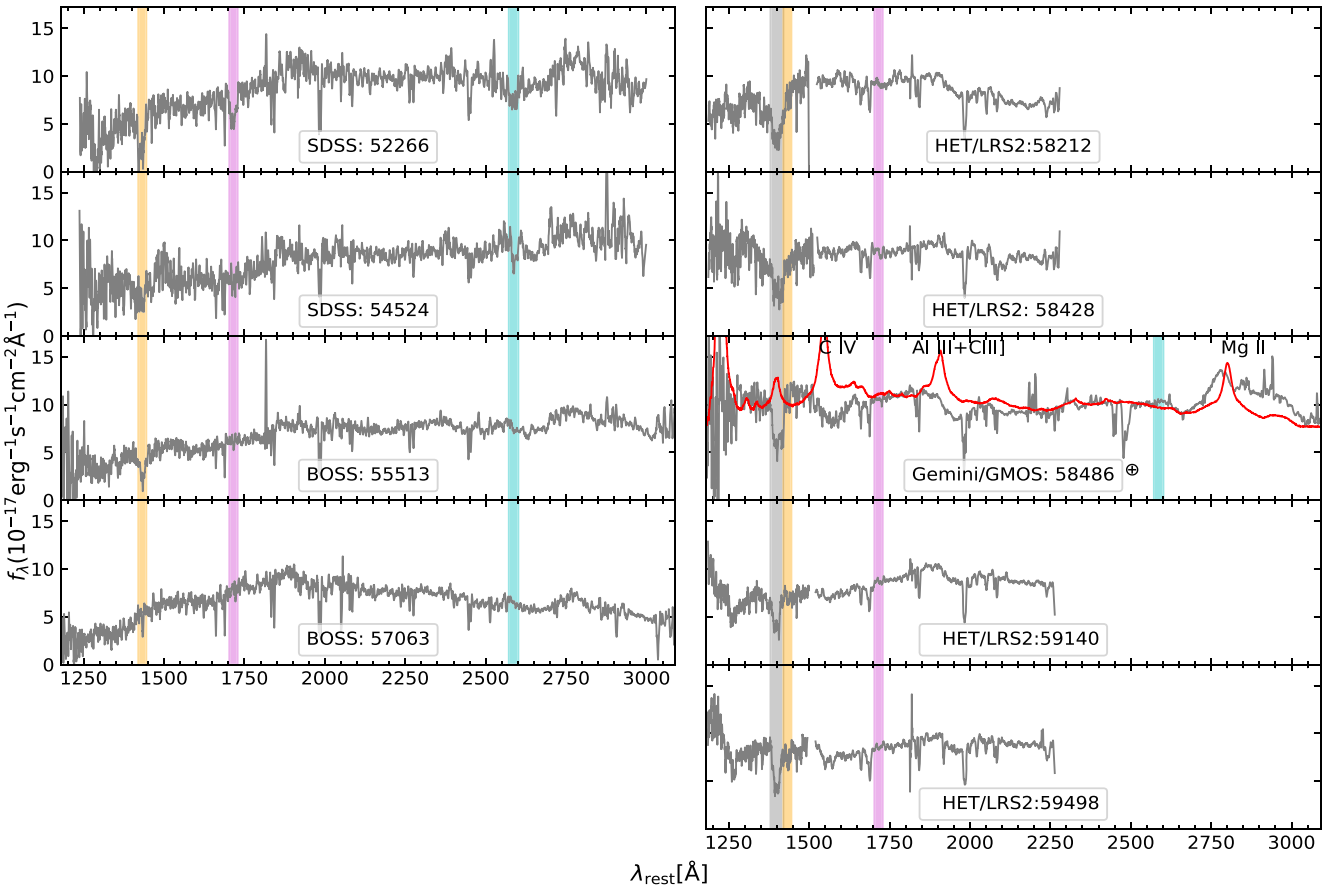


**Figure 3.** All the optical spectra (smoothed by a 15 pixel Savitzky–Golay filter) obtained by SDSS, Gemini/GMOS, and HET/LRS2. The cyan, magenta, and orange shadings refer to the Mg II, Al III, and C IV BALs at the same LOS velocity range while the gray shading depicts the newly emerged C IV BAL at a higher LOS velocity. The red spectrum is the normal quasar composite from Vanden Berk et al. (2001) reddened by an unusual extinction curve from Jiang et al. (2013) to match the spectrum at MJD = 58,486; the plus is for telluric absorption. It is clear that the Mg II/Al III LoBALs (cyan/magenta shadings) completely disappeared at MJD = 57,063 and never reappeared in later epochs, while a HiBAL (gray shadings) emerged rapidly and is persistent after MJD = 57,063. During the LoBAL → HiBAL transformation, the quasar continuum becomes progressively bluer in the later epoch while its C IV emission remains weak.

As reported in Yi et al. (2019b), one conspicuous feature is that the low-velocity C IV, Al III, and Mg II BALs at the same LOS velocity slowly weakened until they completely disappeared after MJD = 57,063, then a stronger C IV BAL (gray shading) emerges abruptly (<1 rest-frame yr) at a higher velocity (see Figure 4). The simultaneous BAL disappearance/emergence along with such a dramatic velocity shift over less than one rest-frame year robustly rule out BAL acceleration across the entire trough, although acceleration may occur in some BAL subunits, a scenario that cannot be assessed using the data. Our recent two HET/LRS2 observations confirm the persistence of the newly emerged C IV BAL at $v_{\rm LOS} \approx 0.1c$. In addition, there is a large decrease in BAL-trough width from MJD = 58,486 to 59,140, such that the red-wing (low-velocity) portion of this BAL trough disappeared (see Figure 4); then, the BAL strength appears to level off after MJD = 59,140. The nonzero-flux, flat-bottom portion of BALs is indicative of patchy/clumpy outflows partially covering its background light source (e.g., Veilleux et al. 2016; Hamann et al. 2019).

A careful examination of Figure 3 reveals another two notable variability behaviors. First, the last three-epoch spectra clearly show that the LoBAL species (Al III and Mg II) disappeared and never returned after MJD = 57,063, confirming the LoBAL → HiBAL transformation. The lack of Al III BALs seen from the HET/LRS2 spectra is a strong indicator of the absence of Mg II BALs, as both BAL species vary nearly hand in hand based on investigations of the LoBAL sample (see Figure 18 in Yi et al. 2019a; also see Figure 4). Second, the continuum shape becomes progressively bluer in later epochs, suggesting a rapid decrease of dust along our LOS during the LoBAL → HiBAL transformation.

We conclude that this quasar provides an excellent example of BAL transformations fitting the evolutionary path from red to blue quasars. Such a transformation may occur many times over the entire quasar lifetime. Longer-timescale monitoring is required to confirm whether it is an episodic or a permanent transformation.

### 3.4.2. Variability in the BELs

In this subsection, we explore the variability of the BELs, whose behavior may provide useful diagnostics in assessing subsequent BAL variability after the LoBAL → HiBAL transformation and shed light on the nature of WLQs (e.g., Diamond-Stanic et al. 2009; Plotkin et al. 2015).

According to the large difference in systemic redshift measured by Mg II and H$\beta$ (see Section 3.1), the Mg II BEL appears to be blueshifted by as much as 2930 km s$^{-1}$ relative to H$\beta$. However, the previous Mg II-based systemic redshift was determined by the relatively low-S/N SDSS spectra. With the aid of a higher-quality spectrum from Gemini/GMOS, we are now able to more precisely locate the peak of the Mg II BEL at

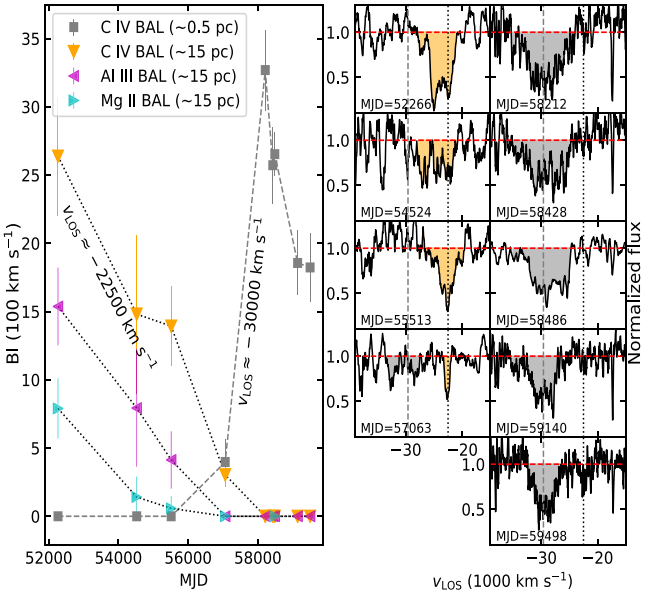


**Figure 4.** Left panel: Time-variability of different-velocity, different-ion BALs, in which the C IV (gray squares and orange triangles), Al III (magenta triangles), and Mg II (cyan triangles) BALs are indicated. Right panel: The corresponding BAL-profile variability over the sampling epochs. Mg II and Al III BAL profiles are not displayed here to avoid overcrowding (see the color shadings in Figure 3). The filled orange/gray colors depict the BAL disappearance/emergence processes in time series (left) and velocity space (right). The LoBAL and HiBAL absorbers are located at ∼15 and ∼0.5 pc from its SMBH (see Yi et al. 2019b), with the characteristic velocities marked by the gray dotted and dashed lines. This quasar can serve as an excellent example of the LoBAL → HiBAL transformation.

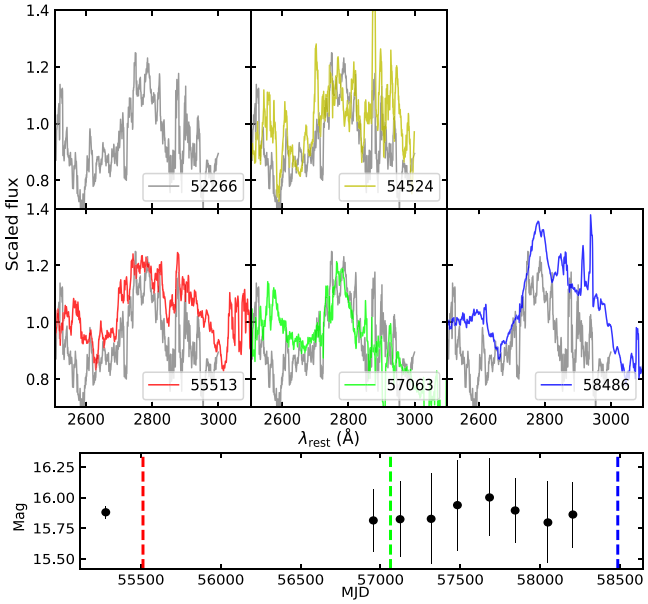


**Figure 5.** Top: The Mg II+Fe II complex emission over the five different epochs, in which each spectrum is scaled to an average flux of the relatively line-free region at $2515 < \lambda_{rest} < 2540$ Å, and the first one is used as a benchmark to guide the eye for variability. The complex emission strengthened substantially from MJD = 57,063 to 58,486. Bottom: The light curve of W1 (NEOWISE Team 2020) shows no significant variability; dashed lines correspond to the above three spectroscopic epochs. The complex emission strengthened by a factor of ∼2 in REW from MJD = 52,266 to 58,486, supportive of an ongoing removal of the dust cocoon.

$\lambda_{rest} = 2780 \pm 5$ Å, which corresponds to $2140 \pm 530$ km s$^{-1}$ in blueshift relative to H$\beta$, one of the largest Mg II blueshifts known to date (e.g., Luo et al. 2015; Plotkin et al. 2015; Rafiee et al. 2016; Venemans et al. 2016; Vito et al. 2021). This value is lower than that derived from the SDSS spectra, partly due to the strengthening in the red wing of the Mg II+Fe II complex emission (see Figure 5). In addition, the C IV BEL remains barely visible, consistent with being classified as a bona fide WLQ. The relatively low-S/N spectra and the small gap at $1500 < \lambda_{rest} < 1520$ Å from the HET/LRS2 spectroscopy make our variability analysis of the C IV BEL in J0827 somewhat uncertain (see Figure 3). Finally, the Ly$\alpha$+N V emission appears to become stronger in later epochs, despite the inability to quantify the variability due to its low S/N on the CCD blue edge. Nevertheless, the variability of BEL highlights the importance of a joint analysis of near-IR and multiepoch optical spectroscopy for J0827.

Another important issue is the underlying link between the BAL and BEL variability. As demonstrated in Figure 4, the low-velocity BALs gradually disappeared from MJD = 52,266 to 58,212, and the high-velocity C IV BAL emerged rapidly after MJD = 57,063. In contrast, the Mg II BEL and the light curve in the W1 band remain generally unchanged from MJD = 57,063 to 58,212, suggesting no significant changes in intrinsic quasar luminosity during this time. Due to the lack of W1 data at MJD > 58,212, we cannot rule out that changes in the incident ionizing flux, a scenario that is hinted at by the decrease of the C IV-BAL BI from MJD = 58,486 to 59,140, play a (secondary) role in the strengthening of the complex emission from MJD = 57,063 to 58,486, despite transverse motion dominating the BAL transformation. The true situation, however, could be much more complicated given the following reasons: (1) the observed LoBAL disappearance along with a large decrease in continuum reddening strongly supports an ongoing removal of its dust cocoon; (2) BELs and BALs signal the bulk and single-LOS effects, respectively, therefore changes in BAL may not necessarily accompany changes in BEL, particularly when considering patchy/dusty LoBAL winds; and (3) the composition and distribution of dust in J0827 remain largely unknown.

## 4. Discussion

We now discuss the implications from joint analyses of the multiepoch optical spectra sampled over two decades and near-IR spectroscopy, as well as mid-IR photometry for J0827.

### 4.1. Implications from the BAL Winds

Because BAL winds are believed to be launched from a rotating accretion disk and then accelerated by radiation pressure (e.g., Proga et al. 2000; Grier et al. 2016), it is reasonable to assume that the observed LoBAL disappearance is caused by transverse motion with a velocity comparable to the Keplerian velocity. As reported in Yi et al. (2019b), the LoBAL/HiBAL distances in J0827 were estimated to be $R \sim 15/\sim 0.5$ pc from its SMBH, with roughly an order-of-magnitude uncertainty. The LoBAL distance is consistent with interferometric observations of local active galactic nuclei (e.g., Hönig et al. 2013) and the finding from Ricci et al. (2017). Therefore, the kinetic power ($\dot{E}_k = 2\pi R \Omega \mu m_p N_H v^3$) for the LoBAL wind is estimated to be $3.45 \times 10^{46}$ erg s$^{-1}$ (∼43% of the Eddington luminosity), when adopting a hydrogen column density $N_H = 10^{22}$ cm$^{-2}$ and a global covering factor $\Omega = 0.5$ (both are the lower limits for LoBAL quasars; e.g., Boroson & Meyers 1992; Gallagher et al. 2006; Gibson et al. 2009;

Urrutia et al. 2009; Hamann et al. 2019) and a characteristic velocity of $2.25 \times 10^9$ cm s$^{-1}$ (see Figure 4). Such a powerful wind, in principle, is capable of expelling circumnuclear material to galactic/circumgalactic scales. Even if the BAL-wind kinetic power is an order of magnitude lower (~5% of the Eddington luminosity), its host galaxy could still be substantially affected by the BAL wind, if provided with a coupling efficiency of $\gtrsim$10% between the BAL wind and interstellar medium (ISM; see Hopkins & Elvis 2010).

Besides the powerful LoBAL wind at $R \sim 15$ pc from the SMBH, there is a HiBAL wind arising at a region whose size ($R \sim 0.5$ pc) is comparable to that of the BLR (e.g., Grier et al. 2017 and references therein), which may ultimately clear out the remnant circumnuclear dust/gas and speed the transition of a red quasar into a blue quasar. This scenario, of course, cannot be directly tested by the optical spectra of J0827 spanning only two decades, but we do see some evidence from its parent sample, which can be summarized as follows: (1) Yi et al. (2019a) discovered that weakening BALs outnumber strengthening BALs on longer sampling timescales in the LoBAL sample; (2) Yi & Timlin (2021) further revealed that the remarkable time-dependent variability in LoBALs described above occurs in the regime where quasars become bluer in later epochs (see Figure 4 in that work); and (3) all six LoBAL quasars undergoing LoBAL → HiBAL/non-BAL transformations in Yi & Timlin (2021) became bluer in later epochs. Together with the broad range of striking properties observed in J0827, we suggest that LoBAL quasars such as J0827 could be caught in the act of casting off their dust cocoons, given that LoBALs have high column densities and are almost certainly associated with dust and that the inclination is likely intermediate or possibly closer to its polar axis due to the type 1 quasar nature.

There are interesting implications of the two different-scale BAL winds located at $R \sim 0.5$ and $R \sim 15$ pc from the quasar center. Recent observational studies based on large samples suggest that the majority of BAL winds are distributed in a wide distance range, i.e., at $R \sim$ 10–1000 pc from their SMBHs (e.g., Arav et al. 2018; He et al. 2019). Such a wide distribution of BAL-wind scales can be better understood in the evolutionary path from red to blue quasars, given that J0827 is a LoBAL quasar surrounded by a heavy dust cocoon while these samples mainly consist of HiBAL quasars whose dust cocoons have been mostly dispersed by previous winds. This path is supported by (1) the overall LoBAL → HiBAL transformation sequence along with a decrease in reddening observed from the LoBAL sample (Yi & Timlin 2021), and (2) the larger-distance BAL wind having a lower LOS velocity observed in J0827 (see Figure 4), although we did not detect evident acceleration signatures in this quasar. However, nondetection of BAL-acceleration signatures over the nine epochs could be due to the saturation effect indicated by the nonzero-flux, flat-bottom portions of the BALs, the blending of numerous subunits across a BAL trough, the short time span (7 rest-frame yr) compared to a typical BAL lifetime of at least hundreds of years (e.g., Filiz Ak et al. 2013; Yi & Timlin 2021), and/or the insufficient spectral quality.

Indeed, we find evidence of BAL acceleration in a few brighter quasars accompanying a conspicuous decrease or even complete disappearance of LoBAL species in an ongoing study. Observations of these quasars may offer valuable clues for the open, extremely challenging question—how do quasar winds travel from nuclear to galactic scales? Given the near-Eddington accretion and dusty/patchy LoBAL wind observed in J0827, radiation pressure on dust likely plays an important role in the feedback of momentum and energy from nuclear to galactic scales for this process, in agreement with the predictions from some theoretical works (e.g., Fabian et al. 2008; Costa et al. 2014; Giustini & Proga 2019) and observational studies (e.g., Ricci et al. 2017; Coatman et al. 2019; Leftley et al. 2019; Yi et al. 2020). We also aim to explore the BAL–ISM coupling process from an excellent later-phase analog of J0827, another brighter/bluer WLQ at $z \sim 2$ showing BAL deceleration, weak radio emission at 1.4 GHz, excess emission at $\lambda_{\rm rest} = 7.5$ $\mu$m, and multiscale/multiphase outflows, in a future study. Such investigations may help to reveal the origin of quasar reddening and shed light on the lack of significant differences in emission-line outflows between red and blue quasars (see below).

### 4.2. Implications from the SED

The most dramatic feature seen from Figure 1 is that the observed SED of J0827 is in good agreement with the scaled normal quasar SED only at $\lambda_{\rm rest} > 0.4$ $\mu$m but deviates increasingly at $\lambda_{\rm rest} < 0.3$ $\mu$m. Although the SMC extinction curve has been widely adopted in the literature for studies of quasar dust properties, it cannot explain such behavior in J0827, unless with a break at $\lambda_{\rm rest} \sim 0.3$ $\mu$m. In contrast, the anomalous extinction curve from Jiang et al. (2013) can satisfactorily reproduce this behavior without the need to invoke two extinction curves at $\lambda_{\rm rest} \lesssim 0.3$ $\mu$m and $\lambda_{\rm rest} \gtrsim 0.3$ $\mu$m. From a physical perspective, quasar activities can cause the destruction of large dust grains or in situ formation of dust grains may occur in quasar winds. The extinction curve from Jiang et al. (2013) is an optimal choice to fit the entire SED for J0827, provided that its intrinsic SED is closely similar to the normal quasar SED.

A number of observational studies have reported significant correlations between C IV BEL/BAL properties (i.e., blueshift and EW) and dust properties traced by rest-frame 2–6 $\mu$m emission and UV/NIR spectral slopes (e.g., Zhang et al. 2014; Baron & Netzer 2019; Rankine et al. 2020; Yi et al. 2020; Temple et al. 2021), suggestive of an underlying link between quasar wind and dust across 1–1000 pc scales. However, these studies suffered from large uncertainties in distance for both wind and dust, making robust assessments difficult. For example, Yi et al. (2020) found significant differences in the narrow-line region and BLR kinematics between the BAL and non-BAL samples matched in redshift and luminosity, such that BAL quasars tend to have larger C IV and [O III] blueshifts. Similarly, Calistro Rivera et al. (2021) discovered a higher incidence of outflow signatures traced by large C IV-BEL blueshifts and broad [O III] wings in red quasars compared to their control sample, implicating pc- and kpc-scale dusty winds as a potential key ingredient for red quasars. In contrast, some studies found no significant differences in outflow properties between red and blue quasars matched in luminosity (e.g., Temple et al. 2019; Villar Martín et al. 2020; Fawcett et al. 2022). The apparent discrepancy could be due primarily to the difference in sample size and/or the specific fitting methods, such as the difficulties in decomposing robust [O III] kinematics from type 1 quasar spectra (e.g., Coatman et al. 2019; Villar Martín et al. 2020). Therefore, unambiguous quasar winds like BALs, particularly those with a good constraint on the wind

distance, provide valuable diagnostics to study the underlying link between wind and dust.

Fortunately, the remarkable BAL transitions of J0827 allow us to constrain its LoBAL wind distance at $R \sim 15$ pc from the quasar center (see Yi et al. 2019b). In combination with the estimated kinetic power (~43% of the Eddington luminosity) of the LoBAL wind, the strengthening in Mg II emission suggestive of dust removal, and a large decrease of reddening after the LoBAL → HiBAL transformation, it is likely that this quasar is caught in the act of casting off its dust cocoon located at $R \sim 15$ pc, with an outermost shell perhaps extending to $R \sim 1000$ pc. We conclude that J0827 offers a clear example of dusty winds as the origin of quasar reddening, which, in turn, supports the excess emission at $\lambda_{\rm rest} = 7.0\ \mu$m (e.g., Baron & Netzer 2019; Calistro Rivera et al. 2021).

### 4.3. A Potential Link between WLQs and BAL Quasars

The majority of WLQs known to date have been identified from single-epoch spectroscopy; in addition, the current WLQ samples targeted at X-ray wavelengths exclude quasars with apparent absorption features (e.g., Wu et al. 2012; Luo et al. 2015; Ni et al. 2018), making the link to outflows unclear. While Plotkin et al. (2015) proposed a "wind-dominated" scenario for typical non-BAL WLQs on the basis of their BEL properties, there is some debate if winds are traced by emission lines (e.g., Gaskell 1982; Richards et al. 2011; Villar Martín et al. 2020; Zuo et al. 2020). Recently, Ni et al. (2018) invoked a thick disk+outflow model for WLQs, but they implicitly considered both components as the shield material and did not consider the impact of disk winds on the circumnuclear or larger-scale environment. Therefore, the connection between WLQs and outflow properties remains largely unexplored in these studies. In this context, searching for unambiguous quasar winds like BALs among WLQs is particularly valuable.

Rogerson et al. (2016) reported a dramatic non-BAL → HiBAL transformation in a quasar J0230, which was considered to be a WLQ due to the persistence of extremely weak C IV emission over one decade. Similarly, from our ongoing spectroscopic campaign on quasars showing BAL transitions, we discovered a more surprising phenomenon: a WLQ is undergoing multiple HiBAL ⇌ non-BAL transformations over two decades in an ongoing study. In addition, Jiang et al. (2013) demonstrated that the C IV BEL of their LoBAL quasar remains weak after the correction for internal reddening (see Figure 5 in their work). Likewise, the C IV BEL in J0827 is much weaker than that from the quasar composite reddened by the same reddening curve from Jiang et al. (2013) to match the continuum level of J0827 (see Figure 3). Moreover, J0827 is undergoing a LoBAL → HiBAL transformation and its C IV BEL appears barely visible over all the spectroscopic epochs; in particular, the optical spectrum at MJD = 57,063 did not show conventional BAL features and remained barely visible in the C IV BEL, making it a bona fide WLQ. The nearest quasar, Mrk 231 (Veilleux et al. 2016), resembles J0827 in many aspects, such as weak high-ionization BELs compared to normal H$\alpha$ emission, LoBAL winds at $R \sim 2$–20 pc, large BEL blueshift, weak or absent [O III] emission, near-Eddington-ratio accretion, a sudden spectral turning point at $\lambda_{\rm rest} \sim 0.3\ \mu$m, a peak of the SED at $\lambda_{\rm rest} \sim 7\ \mu$m, and a time-variability pattern characterized by a rapid rise and a slow decline in BAL strength (Lípari et al. 2005). Intriguingly, Leighly et al. (2014) reported tentative evidence for BAL deceleration in Mrk 231, a telltale sign of the BAL–ISM coupling in action. These results indicate WLQs having BAL and dust features are an important population to bridge the gap between red and blue WLQs, presumably because BAL winds play a role in shedding dust cocoons (see Section 4.1). In agreement with Yi & Timlin (2021), the above five WLQs, among which three are LoBAL quasars that are much redder than the other two HiBAL quasars, together fit the predominant LoBAL → HiBAL/non-BAL transformation sequence along with a decrease in the amount of dust, further supporting the evolutionary path of red quasars transitioning into blue quasars. Weak, narrow absorption lines (NALs) may be more prevalent in WLQs than previously thought (Paul et al. 2022), but we do not discuss this issue due to the difficulty of identifying quasar outflows traced by NALs.

Almost all WLQ studies have not explored the time-variability of BELs. Through visual inspection of objects with multiepoch SDSS spectra in two previous WLQ studies, we found that the "pristine" WLQs from Luo et al. (2015) vary more frequently and dramatically than the "bridge" population of WLQs from Ni et al. (2018) with respect to emission, absorption, and/or continuum properties, i.e., 4 out of 17 quasars with multiepoch spectra from Luo et al. (2015) show appreciable variability of the C IV BEL in REW as opposed to non-such cases in the bridge quasars from Ni et al. (2018). In contrast, the multiepoch optical spectroscopy of J0827 reveals that both the Mg II and C IV BELs strengthened along with a decrease of the Mg II blueshift in later epochs. Thus, our initial investigation of variability in BEL between WLQs and bridge quasars suggests a one-way direction, such that bona fide WLQs transition into the bridge population (similar to the LoBAL → HiBAL/non-BAL sequence mentioned above), hinting that WLQs may be at an earlier phase than the bridge quasars. However, we caution about a potential (though unlikely) bias due to the lack of a thorough examination for normal quasars transitioning into WLQs. Such a transition, to our knowledge, has not been reported but might occur, i.e., Ross et al. (2020) found 3 out of 64,774 quasars exhibit dramatic changes in the C IV BEL, although none of them has C IV REWs less than 15 Å at any sampling epochs. Nevertheless, the persistence of a large Mg II blueshift (see Section 3.4.2) and weak C IV emission (see Figure 3) in J0827 suggests that this quasar may still have to spend a considerable time (perhaps a few million years) before evolving into a normal, blue quasar.

Our spectral fitting for J0827 reveals a rapid accretion state ($\lambda_{\rm Edd} \sim 0.71$), supporting the argument that WLQs may be in an exceptionally high accreting phase, i.e., near- or super-Eddington accretors (e.g., Luo et al. 2015; Veilleux et al. 2016; Ni et al. 2018). This interpretation is supported by the potential excess emission at $\lambda_{\rm rest} \approx 7\ \mu$m as justified in Section 4.2, which may lead to an underestimation of the bolometric luminosity, although the excess could be contributed predominantly by dusty outflows (e.g., Hönig et al. 2013; Zakamska & Greene 2014; Baron & Netzer 2019). Combined with all the H$\beta$-based Eddington ratios larger than 0.3 found in a non-BAL WLQ sample from Plotkin et al. (2015), makes it tempting to conclude that WLQs have near- or super-Eddington ratios with accompanying thick disks (e.g., Wang et al. 2014; Luo et al. 2015; Veilleux et al. 2016; Ni et al. 2018; Giustini & Proga 2019). Likewise, high-$z$ BAL quasars tend to possess near- or super-Eddington ratios estimated by H$\beta$ and Mg II (e.g., Wang et al. 2018; Yi et al. 2020). Therefore, a

high-Eddington ratio ($\gtrsim$0.3) may be a fundamental quantity in connecting both the WLQ and BAL populations. We briefly outline this argument below.

Previous studies of WLQs, mainly from an X-ray perspective, suggest a "shielding" scenario (e.g., Wu et al. 2012; Luo et al. 2015; Ni et al. 2018). Similarly, some BAL models also require a "shielding" mechanism by which high-energy photons are blocked from reaching the UV absorbers (e.g., Proga et al. 2000). From an observational view, both WLQs and BAL quasars with weak BELs favor a soft ionizing SED (e.g., Plotkin et al. 2015; Hamann et al. 2019; Rankine et al. 2020; Paul et al. 2022), consistent with the prediction from shielding. Such shielding would naturally produce high-velocity outflows, which is supported by the prevalence of large C IV BEL blueshifts seen in WLQs and subrelativistic winds observed in BAL quasars (e.g., Luo et al. 2015; Yi et al. 2019a; Rankine et al. 2020). Additionally, weak narrow-core [O III] emission is often seen in LoBAL quasars and WLQs (e.g., Boroson & Green 1992; Wu et al. 2011; Plotkin et al. 2015; Yi et al. 2020), in agreement with shielding. Indeed, shielding lends support to the argument that BEL blueshift, BAL, and perhaps broad [O III] emission could be different manifestations of the same quasar-driven outflow system (e.g., Rankine et al. 2020; Xu et al. 2020; Yi et al. 2020; Liu et al. 2021), presumably because shielding plays a key role in producing powerful disk winds that can travel out to large scales. In contrast, the LoBAL wind and weak BELs/narrow-core [O III] emission are indicative of shielding. Therefore, in the context of shielding resulting from high-Eddington accretion, the WLQ, BAL, and weak narrow-core [O III] emission may be unified for J0827. However, realistic shielding could be much more complicated than the discussion here (e.g., Nenkova et al. 2008; Ricci et al. 2017; Ni et al. 2020), as the nature of the shielding material remains unknown.

## 5. Summary and Future Work

The main results and implications from joint analyses of the multiwavelength data are concluded as follows.

1. The systemic redshift of J0827 is measured to be $z = 2.070 \pm 0.001$ using H$\beta$, significantly larger than the Mg II-based one ($z = 2.040 \pm 0.003$) reported in the literature. Our measurements yield an extreme Mg II blueshift of $2140 \pm 530$ km s$^{-1}$ relative to H$\beta$ (see Section 3.1).
2. Based upon the single-epoch scaling relation, the BH mass and Eddington ratio are estimated to be $M_{\rm BH} = 6.1 \times 10^8 M_\odot$ and $\lambda_{\rm Edd} = 0.71$, with a typical uncertainty of 0.3 dex (see Section 3.3).
3. The LoBAL wind is thought to be located at $R \sim 15$ pc from its BH. Combined with the type 1 quasar nature, J0827 fits better to a dust cocoon than the conventional torus. Adopting typical values of the global covering factor (0.5) and hydrogen column density ($10^{22}$ cm$^{-2}$) in LoBAL quasars, the wind kinetic power is estimated to be 43% of the Eddington luminosity with an order-of-magnitude uncertainty. J0827 provides an excellent laboratory to test the evolutionary path from red to blue quasars, given the (episodic) LoBAL → HiBAL transformation along with a rapid decrease in reddening characteristic of the blowout phase (see Section 4.1).
4. Our analyses support the presence of excess emission at rest-frame 7 $\mu$m for J0827 compared to normal quasars, on the basis of dusty outflows traced by the powerful LoBAL wind (see Section 4.2).
5. Based upon a visual inspection of variability among the five WLQs with BALs, typical WLQs without BALs, and bridge quasars, WLQs tend to vary more frequently and dramatically than the bridge quasars in emission, absorption, and continuum (see Section 4.3).
6. Our investigations of J0827 complement the "wind-dominated" scenario invoked for WLQs and suggest that both WLQs and BAL (particularly LoBAL) quasars favor soft ionizing SEDs and high-Eddington ratios and that the WLQ, BAL, and weak narrow-core [O III] emission phenomena may be unified in the broad context of shielding for this quasar (see Section 4.3).

It is well established that LoBAL quasars are considerably redder than HiBAL/non-BAL quasars and that the BAL fraction is much higher in red quasars than in blue quasars. While leading models of galaxy formation predict an evolutionary path from red to blue quasars, solid observational evidence remains lacking, perhaps due to the short-lived nature of red quasars. As a case study, the observed LoBAL → HiBAL transformation in J0827, along with the LoBAL wind at $R \sim 15$ pc and a large decrease in reddening over two decades, provides a unique opportunity to demonstrate that BAL winds play a critical role in transforming red quasars into blue quasars via the rapid removal of their dust cocoons. Therefore, J0827 can serve as an excellent example of BAL winds destroying dust/gas cocoons, a scenario that has long been invoked by observational and theoretical studies. Furthermore, we will test this scenario in detail in combination with other quasars showing BAL transformations and acceleration signatures in the future.

In addition, longer time baseline and wider wavelength coverage observations of J0827 can trace its time evolution, constrain the star formation rate, explore the radio emission, study the dust properties, and further assess whether this quasar is at the end of the blowout phase toward unveiling a blue quasar or just reflects an episodic ignition of quasar activities from a dusty environment.

We thank the anonymous referee for constructive feedback that helped improve this manuscript. We are grateful to Robin Ciardullo and Michael Eracleous for assistance with the observations by the Hobby-Eberly Telescope. W.Yi, W.N.B., and Q.N. acknowledge support from NSF grant AST-2106990, CXC grant GO0-21080X, and the V.M. Willaman Endowment at Penn State. W.Yi is also grateful for support from the National Science Foundation of China (11703076) and the West Light Foundation of The Chinese Academy of Sciences (Y6XB016001). L.C.H. was supported by the National Science Foundation of China (11721303, 11991052) and the National Key R&D Program of China (2016YFA0400702). B.L. acknowledges financial support from the National Natural Science Foundation of China grant 11991053. W.Yi, X.-B.W., and J.-M.B. acknowledge the science research grants from the China Manned Space Project with No. CMS-CSST-2021-A06. J.-M.B. acknowledges the National Natural Science Foundation of China grant 11991051.

This work uses data obtained from the Gemini Observatory (PI: Yi; program ID: GN-2018B-FT-214 and GN-2020A-FT-203), which is operated by the Association of Universities for Research in Astronomy, Inc., under a cooperative agreement with the NSF on behalf of the Gemini partnership: the National

Science Foundation (United States), the National Research Council (Canada), CONICYT (Chile), Ministerio da Ciencia, Tecnologia e Inovaciao (Brazil) and Ministerio de Ciencia, Tecnologia e Innovacion Productiva (Argentina). This research also uses data obtained through the Telescope Access Program (TAP), which has been funded by the National Astronomical Observatories of China, the Chinese Academy of Sciences (the Strategic Priority Research Program "The Emergence of Cosmological Structures" grant No. XDB09000000), and the Special Fund for Astronomy from the Ministry of Finance. Observations obtained with the Hale Telescope at Palomar Observatory were obtained as part of an agreement between the National Astronomical Observatories, the Chinese Academy of Sciences, and the California Institute of Technology. The Hobby-Eberly Telescope (HET) is a joint project of the University of Texas at Austin, the Pennsylvania State University, Ludwig-Maximillians-Universität München, and Georg-August-Universität Göttingen. The Hobby-Eberly Telescope is named in honor of its principal benefactors, William P. Hobby and Robert E. Eberly. The Low-Resolution Spectrograph 2 (LRS2) was developed and funded by the University of Texas at Austin McDonald Observatory and Department of Astronomy, and by the Pennsylvania State University. We thank the Leibniz-Institut für Astrophysik Potsdam and the Institut für Astrophysik Göttingen for their contributions to the construction of the integral field units. Funding for SDSS-III has been provided by the Alfred P. Sloan Foundation, the Participating Institutions, the National Science Foundation, and the US Department of Energy Office of Science.

## ORCID iDs

Weimin Yi https://orcid.org/0000-0001-9314-0552
W. N. Brandt https://orcid.org/0000-0002-0167-2453
Q. Ni https://orcid.org/0000-0002-8577-2717
Luis C. Ho https://orcid.org/0000-0001-6947-5846
Bin Luo https://orcid.org/0000-0002-9036-0063
D. P. Schneider https://orcid.org/0000-0001-7240-7449
Jeremiah D. Paul https://orcid.org/0000-0003-0040-3910
Richard M. Plotkin https://orcid.org/0000-0002-7092-0326
Jinyi Yang https://orcid.org/0000-0001-5287-4242
Feige Wang https://orcid.org/0000-0002-7633-431X
Zhicheng He https://orcid.org/0000-0003-3667-1060
Chen Chen https://orcid.org/0000-0002-6258-721X
Xue-Bing Wu https://orcid.org/0000-0002-7350-6913

## References

Allen, J. T., Hewett, P. C., Maddox, N., Richards, G. T., & Belokurov, V. 2011, MNRAS, 410, 860
Arav, N., Liu, G., Xu, X., et al. 2018, ApJ, 857, 60
Banerji, M., Alaghband-Zadeh, S., Hewett, P. C., et al. 2015, MNRAS, 447, 3368
Baron, D., & Netzer, H. 2019, MNRAS, 482, 3915
Boroson, T. A., & Green, R. F. 1992, ApJS, 80, 109
Boroson, T. A., & Meyers, K. A. 1992, ApJ, 397, 442
Calistro Rivera, G., Alexander, D. M., Rosario, D. J., et al. 2021, A&A, 649, A102
Chonis, T. S., Hill, G. J., Lee, H., et al. 2014, Proc. SPIE, 9147, 91470A
Coatman, L., Hewett, P. C., Banerji, M., et al. 2019, MNRAS, 486, 5335
Costa, T., Sijacki, D., & Haehnelt, M. G. 2014, MNRAS, 444, 2355
Davis, B. D., Ciardullo, R., Jacoby, G. H., et al. 2018, ApJ, 863, 189
De Cicco, D., Brandt, W. N., Grier, C. J., et al. 2018, A&A, 616, A114
Diamond-Stanic, A. M., Fan, X., Brandt, W. N., et al. 2009, ApJ, 699, 782
Du, P., Hu, C., Lu, K.-X., et al. 2014, ApJ, 782, 45782/1/45
Fabian, A. C., Vasudevan, R. V., & Gandhi, P. 2008, MNRAS, 385, L43
Fan, X., Strauss, M. A., Gunn, J. E., et al. 1999, ApJL, 526, L57
Fawcett, V. A., Alexander, D. M., Rosario, D. J., et al. 2022, MNRAS, in press
Filiz Ak, N., Brandt, W. N., Hall, P. B., et al. 2013, ApJ, 777, 168
Fynbo, J. P. U., Krogager, J.-K., Venemans, B., et al. 2013, ApJS, 204, 6
Gallagher, S. C., Brandt, W. N., Chartas, G., et al. 2006, ApJ, 644, 709
Gaskell, C. M. 1982, ApJ, 263, 79
Gibson, R. R., Jiang, L., Brandt, W. N., et al. 2009, ApJ, 692, 758
Giustini, M., & Proga, D. 2019, A&A, 630, A94
Glikman, E., Helfand, D. J., & White, R. L. 2006, ApJ, 640, 579
Glikman, E., Urrutia, T., Lacy, M., et al. 2012, ApJ, 757, 51
Greene, J. E., & Ho, L. C. 2005, ApJ, 630, 122
Grier, C. J., Brandt, W. N., Hall, P. B., et al. 2016, ApJ, 824, 130
Grier, C. J., Trump, J. R., Shen, Y., et al. 2017, ApJ, 851, 21
Hamann, F., Herbst, H., Paris, I., & Capellupo, D. 2019, MNRAS, 483, 1808
He, Z., Wang, T., Liu, G., et al. 2019, NatAs, 3, 265
Hill, G. J., Lee, H., MacQueen, P. J., et al. 2021, ApJ, 162, 298
Hönig, S. F., Kishimoto, M., Tristram, K. R. W., et al. 2013, ApJ, 771, 87
Hopkins, P. F., & Elvis, M. 2010, MNRAS, 401, 7
Indahl, B., Zeimann, G., Hill, G. J., et al. 2019, ApJ, 883, 114
Jiang, P., Zhou, H., Ji, T., et al. 2013, AJ, 145, 157
Leftley, J. H., Hönig, S. F., Asmus, D., et al. 2019, ApJ, 886, 55
Leighly, K. M., Terndrup, D. M., Baron, E., et al. 2014, ApJ, 788, 123
Lípari, S., Terlevich, R., Zheng, W., et al. 2005, MNRAS, 360, 416
Liu, B., Zhou, H.-Y., Shu, X.-W., et al. 2021, RAA, 21, 065
Luo, B., Brandt, W. N., Hall, P. B., et al. 2015, ApJ, 805, 122
Nenkova, M., Sirocky, M. M., Nikutta, R., et al. 2008, ApJ, 685, 160
NEOWISE Team 2020, NEOWISE-R Single Exposure (L1b) Source Table, IPAC, doi:10.26131/irsa144
Ni, Q., Brandt, W. N., Luo, B., et al. 2018, MNRAS, 480, 5184
Ni, Q., Brandt, W. N., Yi, W., et al. 2020, ApJL, 889, L37
Paul, J. D., Plotkin, R. M., Shemmer, O., et al. 2022, ApJ, 929, 78
Plotkin, R. M., Shemmer, O., Trakhtenbrot, B., et al. 2015, ApJ, 805, 123
Proga, D., Stone, J. M., & Kallman, T. R. 2000, ApJ, 543, 686
Rafiee, A., Pirkola, P., Hall, P. B., et al. 2016, MNRAS, 459, 2472
Ramsey, L. W., Adams, M. T., Barnes, T. G., et al. 1998, Proc. SPIE, 3352, 34
Rankine, A. L., Hewett, P. C., Banerji, M., et al. 2020, MNRAS, 492, 4553
Ricci, C., Trakhtenbrot, B., Koss, M. J., et al. 2017, Natur, 549, 488
Richards, G. T., Hall, P. B., Vanden Berk, D. E., et al. 2003, AJ, 126, 1131
Richards, G. T., Kruczek, N. E., Gallagher, S. C., et al. 2011, AJ, 141, 167
Richards, G. T., Lacy, M., Storrie-Lombardi, L. J., et al. 2006, ApJS, 166, 470
Rodríguez Hidalgo, P., Khatri, A. M., Hall, P. B., et al. 2020, ApJ, 896, 151
Rogerson, J. A., Hall, P. B., Ahmed, N. S., et al. 2018, ApJ, 862, 22
Rogerson, J. A., Hall, P. B., Rodríguez Hidalgo, P., et al. 2016, MNRAS, 457, 405
Ross, N. P., Graham, M. J., Calderone, G., et al. 2020, MNRAS, 498, 2339
Schlafly, E. F., & Finkbeiner, D. P. 2011, ApJ, 737, 103
Temple, M. J., Banerji, M., Hewett, P. C., et al. 2019, MNRAS, 487, 2594
Temple, M. J., Banerji, M., Hewett, P. C., et al. 2021, MNRAS, 501, 3061
Timlin, J. D., Brandt, W. N., Ni, Q., et al. 2020, MNRAS, 492, 719
Urrutia, T., Becker, R. H., White, R. L., et al. 2009, ApJ, 698, 1095
Vanden Berk, D. E., Richard, G. T., Bauer, A., et al. 2001, AJ, 122, 549
Veilleux, S., Meléndez, M., Tripp, T. M., et al. 2016, ApJ, 825, 42
Venemans, B. P., Walter, F., Zschaechner, L., et al. 2016, ApJ, 816, 37
Villar Martín, M., Perna, M., Humphrey, A., et al. 2020, A&A, 634, A116
Vito, F., Brandt, W. N., Ricci, F., et al. 2021, A&A, 649, A133
Voit, G. M., Weymann, R. J., & Korista, K. T. 1993, ApJ, 413, 95
Wang, F., Yang, J., Fan, X., et al. 2018, ApJL, 869, L9
Wang, J.-M., Qiu, J., Du, P., et al. 2014, ApJ, 797, 65
Wang, T., Yang, C., Wang, H., et al. 2015, ApJ, 814, 150
Weymann, R. J., Morris, S. L., Foltz, C. B., et al. 1991, ApJ, 373, 23
Wilson, J. C., Henderson, C. P., Herter, T. L., et al. 2004, Proc. SPIE, 5492, 1295
Wright, E. L., Eisenhardt, P. R. M., Mainzer, A. K., et al. 2010, AJ, 140, 1868
Wright, E. L., Eisenhardt, P. R. M., Mainzer, A. K., et al. 2019, AllWISE Source Catalog [Dataset], IPAC, doi:10.26131/irsa1
Wu, J., Brandt, W. N., Anderson, S. F., et al. 2012, ApJ, 747, 10
Wu, J., Brandt, W. N., Hall, P. B., et al. 2011, ApJ, 736, 28
Xu, X., Zakamska, N. L., Arav, N., et al. 2020, MNRAS, 495, 305
Yi, W., Brandt, W. N., Hall, P. B., et al. 2019a, ApJS, 242, 28
Yi, W., & Timlin, J. 2021, ApJS, 255, 12
Yi, W., Vivek, M., Brandt, W. N., et al. 2019b, ApJL, 870, 25
Yi, W., Zuo, W., Yang, J., et al. 2020, ApJ, 893, 95
York, D. G., Adelman, J., Anderson, J. E., et al. 2000, AJ, 120, 1579
Zakamska, N. L., & Greene, J. E. 2014, MNRAS, 442, 784
Zhang, S., Wang, H., Wang, T., et al. 2014, ApJ, 786, 42
Zuo, W., Wu, X.-B., Fan, X., et al. 2020, ApJ, 896, 40